Research Article

Journal of Environmental Nanotechnology

BioRicinus Communis Seed Extract was Used in the Green Manufacture of Zero-valent Iron Nanoparticles for Photocatalyst Elimination of Chromium

Natrayan Lakshmaiya*
Department of Mechanical Engineering, Saveetha School of Engineering, Saveetha Institute of Medical and Technical Sciences (SIMATS), Chennai, TN, India
Received: 22.07.2024 Accepted: 12.09.2024 Published: 30.09.2024
*natrayanphd@gmail.com

ABSTRACT

Zero-valent iron was produced in this work utilising BioRicinus communis seed extract. XRD, SEM, and TEM methods were used to characterise the physicochemical characteristics of the finished products. According to TEM analysis, the iron zero-valent nanomaterials with diameters ranging from 20 to 40 nm and shell-core architectures were successfully produced. XRD findings verified the existence of several organic compounds. The photoactivity of the product was investigated by reducing the contaminant. According to the test result, the inclusion of fruit extract as a nanoscale catalyst in the photocatalyst reduced the hexavalent chromium. According to photocatalyst results, when the particulate dose was 0.675 g/L, the trivalent chromium suffered from low was 100%. A pseudo-second-order solution describes this reaction's kinetics. At pH 3 and 0.5 g/L seed extract concentration, the kinetic rate constant is 0.4. As a result, the frequency of the photocatalyst was significantly increased, and a more significant amount of Cr (VI) was eliminated. The accessible sites became progressively constrained and overloaded with bichromate particles as the starting content of Cr (VI) was increased at a consistent dose. Changing the nanoparticle dosage may considerably boost the reaction rate, hence the effectiveness of a photocatalyst's Cr (VI) catalytic cycle.

Keywords: Bio-synthesis; Valent iron; BioRicinus communis; Microstructural analysis; Hexavalent chromium.

1. INTRODUCTION

Over the last decade, there has been significant research on the production and characterization of nanoparticles (1–100 nm). Nanostructures and nanoparticles may play essential roles in various sectors, including catalysts, pharmacology, energy storage, healthcare, etc. Many people are concerned about the detrimental consequences of climatic changes because of the manufacture, use, and storage of chemical substances used in economic, agricultural, and medicinal processes. Such chemicals, which have a significantly longer lifetime than projected, can penetrate the atmosphere and propagate (Nguyen *et al.* 2020; Nassar *et al.* 2014). Furthermore, pollutants have evolved into a worldwide problem because of their extensive emissions into the environment. Metals, primarily organic matter, aren't biodegradable and can build up in life forms. Such occurrences result in a variety of illnesses and consequences. Chromium is a metallic element that negatively impacts the environment and human beings. This contaminant enters natural streams through industrial wastewater. It is used in surface coatings, colouring, timber preservation, the leather business, metal production, nuclear power plants, and textiles and apparel, among other things. In aqueous systems, the most frequent types of chromite are tetravalent chromite (Cr (III)) and toxic metals (Cr (VI)). Chromium (VI) is the most dangerous aspect, being both poisonous and movable. Trees, mammals, microorganisms, and humans are all harmed by chromium (VI) molecules. Rapid exposure to chrome (VI) can cause diarrhoea and liver problems, among other things; additionally, breathing causes fast drunkenness, stinging, and nose tube irritation (Zhao *et al.* 2016; Wang *et al.* 2014).

Such toxic substances also induce apoptosis, skin rashes, the body's immune system degeneration, allergens, and inflammation of the face, among other things. To avoid the detrimental effects of chromium (VI) on groundwater and environmental health, its content must be reduced before even being released into the atmosphere (Jiang *et al.* 2018; Zangeneh *et al.* 2019). The World Health Organization (WHO) has set the maximum allowable chromium (VI) in bottled water at 60 g/l. In comparison, the United Nations Food and Agriculture Organization (FAO) and the United States Department of Energy (EPA) have set the maximum allowable substances in water supply at 110 g/L. Several technologies such as activated sludge, ozonation, nanofiltration, ozonation, electrical, absorption, and photocatalyst procedures were employed to extract toxic

metals. Recently, there's been a lot of interest in employing photocatalyst techniques to remediate soluble salts by incorporating transistors with the sun's radiation Zhang *et al.* 2019; Omar *et al.* 2014). That approach has a promising basis for decomposing molecules and photocatalyzing the elimination of ions of heavy metals since it is efficient, inexpensive, and ecologically benign. The possibility of using nZVI again for the extraction of various chemicals from freshwater has also been intensively researched in the recent past. Because of its enormous surface region, high reaction rate, and large variety of active spots, nanoparticles could be an efficient and inexpensive molecule for reducing agents. Zero-valent iron nanoparticles are synthesised using two standard techniques.

Each of those processes has disadvantages, notably high costs, the creation of volatile chemicals (hydrocarbons) during the operation, and the harshness of the reduction agent (borohydride). These constraints have motivated scholars to look for answers to this issue. Consequently, the use of green technologies to produce zero-valent iron has increased over the past decade (Huang *et al.* 2018; FOpoku *et al.* 2017). Organic extracts such as foliage and peel are used as corrosion inhibitors in such procedures to reduce tetravalent ferrous metal to zero-valent iron. That approach has various benefits: the utilisation of non-toxic solvent systems and organic ingredients; ii) coating all flavonoids after extraction to minimise agglomeration, stabilise nZVI, and boost the action of nanomaterials; and iii) the extraction of all these chemicals increases the amount of biodegradation (Onwumere *et al.* 2020). Grape branches, Cajanus pentagon, cherry tendrils, wood, tea, peppermint, macher, and hippophage were all employed in biosurfactant production. The investigations' findings revealed that the produced nanomaterials differed in form, structure, and dimension. Furthermore, nanotechnology research shows that iron surfaces are entirely covered by enzymes and tannins, which inhibit nanotechnology degradation. Moreover, the nanomaterials are evenly dispersed in the reaction medium with no particulate clumping. Shahan et al. demonstrated that the structure and shape of eco-friendly nanomaterials differed from the characteristics of chemically generated nanomaterials. Such nanostructures had a surprising performance in terms of extraction yield and length (Haldorai and Shim, 2013).

This research focuses on the eco-friendly synthesis of zero-valent iron nanomaterials using BioRicinus communis seed extract, an African native plant. Unlike other plant-based nanoparticle sources such as wine, black tea, and rhizome leaves, BioRicinus communis seeds are economically unvalued, making them a cost-effective option for nanoparticle synthesis. The use of various plant extracts for nanoparticle production results in different sizes and shapes, affecting their ability to remove toxins from soil and water. In this study, the BioRicinus communis seed extract was employed as both a sealing agent and a protective colloid during nanoparticle formation. The synthesized nanostructures were designed for use as photocatalysts to reduce chromium (VI) in contaminated environments, offering a sustainable approach to environmental remediation.

2. EXPERIMENTAL WORKS

2.1. Materials

The Indian Biochemistry Research Organization in India provided all experimental supplies for this investigation. All of the treatments have been made with double-filtered water. Hydroxide and hydrochloric acid were used to alter the PH. The chromium standard solutions (1 g/L) are made by melting potassium dichromate (2.8292 g) in plain water (1 L). From the standard solutions, different amounts of chromium were produced.

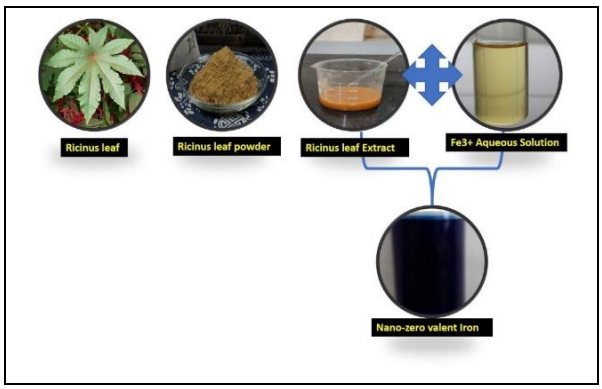

Fig. 1: Bio synthesis of Zero-valent iron nanoparticles from BioRicinus leaf

2.2. Plant Extract Preparations

Clean R. communis samples were gathered from several locations throughout the Adriatic Coast Line, including Al Retrieving Lakes. All seeds were gathered and cleaned frequently with groundwater and rubbing alcohol to eliminate dirt and particle matter. The seeds were then allowed to dry naturally in the open air. Samples were then ripped into tiny chunks using a sterile blade before being ground in a steel grinder to produce a homogenous fine particle (0.5 m), which was then stored in a shaded environment above ambient temperature for future usage. To produce a dark red extraction, a particular amount of seed powder was steeped in filtered water (10% W/V) and carefully swirled at 80°C for 30 minutes. This extract was withdrawn and stirred at 6000 rpm for 15 minutes, while the liquid was filtered through filter paper to remove unwanted content (Samadi *et al.* 2021). The resulting solution was then stored in a freshly sterile, thoroughly dry glass vial in a refrigerator at 5°C for later use.

2.3. Bio Synthesis of Zeo-valent-iron Nanoparticles

In a clean, sterile beaker, combine 10 millilitres of Rc. Drop by drop, seed extract was added to an aqueous phase of Fe3+ ions (6 mL, 0.06 M) with constant swirling. The mixture was then agitated for 20 minutes to improve distribution before being centrifuged for 10 minutes at 13 000 rpm. This black result was then thoroughly rinsed with distilled water and alcohol before being baked inside a furnace at 70°C for 12 hours and designated as Rc. Seed based nanoparticles.

2.4. Specifications of Testing Reactor

For the photocatalyst, a scientific reactor with a capacity of 410 mL and a UVC lamp with moderate pressure and a minimum output of 17 W (Philips) were employed throughout this investigation. The reactor cores inside were composed of borosilicate, and an ultra-violet light with such a crystal coating was installed in the middle. The exterior half of the prototype furnace was built with an entrance at the bottom and an exit at the summit to maintain the average temperature consistent with the air temperature and to allow natural exchange. This reactor contained sample taps employed to gather the necessary sample group at various times. The reactor buildings outside the experiment were constructed of polypropylene and were black to prevent ultraviolet rays from spending energy and conflicting with the illumination within the experiment. The lamps had a spectrum of 243.5 nm, a lifespan of 7000 hours, and an emission output of 250 to 280 W per sq metre at a range of one cm. Its UVC lightbulb was 19.1 cm long and housed under a crystal covering with a circumference of 6 cm that was positioned in the middle of the reactor core.

2.5. Photocatalytic Examination

Research was carried out in a mixed spectrophotometer with a 400-ml optimal capacity. To carry out the experiments, 400 ml of a prepared solution with the required depth was transferred to an experimental setup; then, the generated nanomaterials, such as those of the springboard, were added to the specimen at a therapeutic dose (0.125-0.625 g/L); finally, the UVC lightbulb was positioned inside a crystal cover and immersed in a water solvent, and the setup was instantly powered up. A magnetic stirrer is being used to improve specimen blending. Following the specified time, the specimens were meticulously processed and then used to calculate the quantity of Cr (VI). In this study, the process measures were investigated. The pH was set between 3 and 10, the catalytic dose was 0.131-0.62 g/L, the response period was 5–90 minutes, and the starting Cr (VI) level was 10-200 mg/L. Every phase of an experiment was conducted twice to confirm the findings and the average scores were published. The ideal settings of a parameter were obtained after considering the effectiveness and attaining the perfect circumstances at each step.

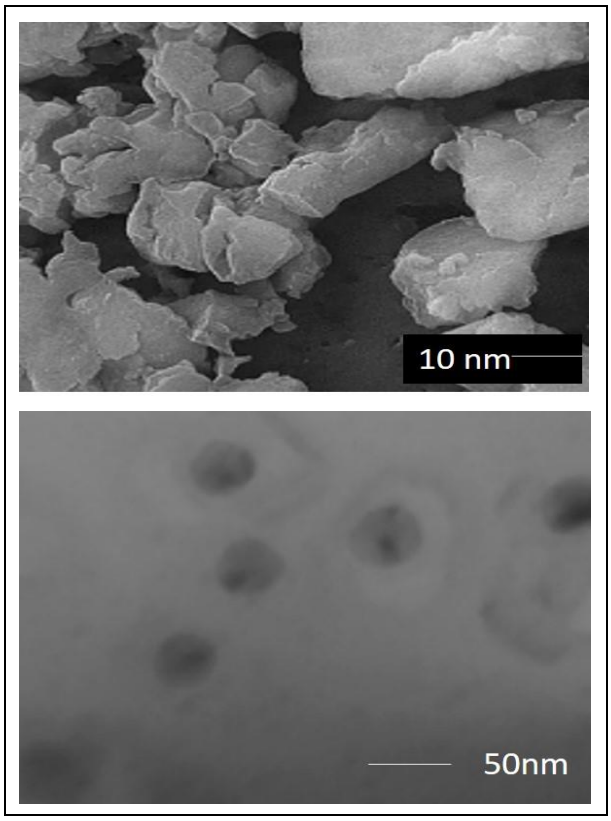

Fig. 2: SEM and TEM images of biosynthesised nanoparticles

2.6. Characterization of Plant Extract

The percentage of Cr (VI) was calculated by observing the interaction of Cr (VI) with 1,5-diphenylcarbazide in an alkaline condition. The absorption of a coloured solution was then determined using a spectrometer at 550 nm. The percentage of Cr (III) in the setup synthetic wastewater output was determined using an atomic absorption to assess the conversion of Cr (VI) to Cr (III). The materials' surface morphologies (physical forms) were determined by scanning electron microscopy coupled with just an energetic linear discrete wavelet for microstructural examinations. Transmission electron microscopy (TEM) was used to assess the size and configuration of the nanoparticles. XRD spectroscopy was also used to evaluate the structure and locate chemical components and bonding.

3. RESULT AND DISCUSSION

3.1. TEM and SEM Analysis

A TEM test was conducted to analyse biologically synthesised nanomaterials' molecular shape and size. Figure 1 depicts the TEM investigation

findings. The TEM pictures illustrate the sphere form of a nanomaterial, which ranged in size from 20 to 40 nm. The protoplanetary disc's uniform and adequate size resulted in nanoparticle absorption during basic pH conditions, while the subshell protected the nanomaterials from oxidising. The structure and form of nanoparticles were examined via SEM examination. The SEM pictures clearly show that perhaps the topology of Rc. seed extract-induced nanomaterials have an uneven shape with certain aggregation (Samadi *et al.* 2021). It is most likely due to the existence of separate categories, such as flavonoids in the seeds.

3.2. XRD Analysis

OriginPro graph plotting software was used in this research to present the results. From Fig. 3 XRD results of zero-valent iron nanostructures showed a strong higher intensity peak at 3 = 42.7°, corresponding to the -FeOOH (111) planes. This is really due to the spherical particles comprising zero-valent nanostructure, according to Li et al. According to scientists, nanoparticles are mainly composed of the core and shell, the oxide layers of iron (II) and iron (III) created by the quick oxidation of ferrous ions in the environment. However, the significant peak at 46.5°, which correlates to a (110) plane, indicates Fe0 (110). Therefore, the characteristic indication at 3 = 43.5° is connected to the square crystal lattice of nanomaterials, as per Standard JCPS Card No. 06 0696.81. These data validate the formation's efficacy. Figure 1 reveals the XRD analysis of nanoparticles.

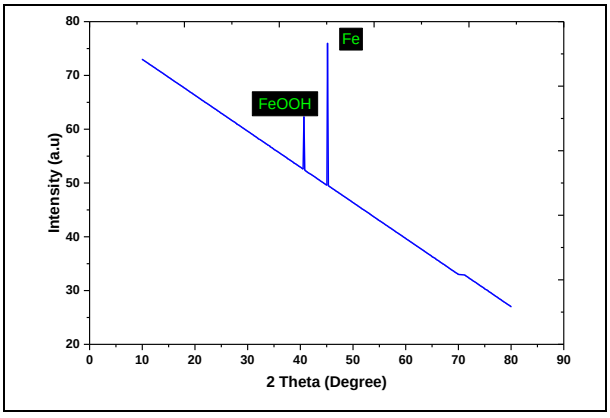

Fig. 3: XRD Pattern of biosynthesised nanoparticles

The high background induced by Fe X-ray photoluminescence might explain the existence of the only nanoscale indication in the XRD pattern. Whenever XRD is used on metal-containing compounds, such as Mn and Fe, the extra X-ray produced by the minerals causes massive radiation levels, disrupting the patterning. Increasing the scanning duration improves the sharpness of the scattered shirts. Moreover, the plants' charcoal on the quantum state surfaces accounts again for 3 distinct peaks at 14.25, 17.86, and 19.59°. Thus, the presence of these different forms demonstrates the importance of bioactive compounds in bio-oxidation along with nanoparticle durability (Nguyen *et al.* 2020).

Such findings demonstrated the importance of crude extract components as caps and reducing and stabilising agents. Clustering is one of the drawbacks of chemical raw nanomaterials. Magnetism agglomeration, van der Waals forces, dissolution at the nanoscale interface, and corroded by-product binding on the material surface all cause such phenomena. That behaviour is a limitation in Cr (VI) to Cr (III) reducing processing equipment because it causes a lack of responsiveness, motility, and inappropriate nanoparticle dispersion. The sustainable particulate production process has mitigated that issue. The coating capability of a polyphenol extraction matrix on zero-valent nanostructured materials promotes nanoparticle durability, minimises nanoparticle agglomeration, extends the response, and boosts the overall reaction. Figure 3 shows the impact of pH on removing Cr (Gupta *et al.* 2014).

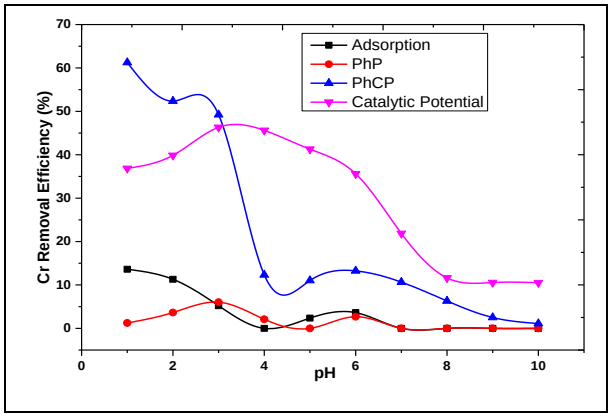

Fig. 4: The impact of solution pH on the removal of Cr

3.3. Catalytic Potential of Valent-iron-Nanoparticles

Over 10 minutes, the figure depicts the effect of varying nanoparticle doses on photocatalyst desorption versus darkness desorption. This photocatalysis with zero dose implies ultraviolet rays lacking photocatalysis, known as the heterogeneous photocatalytic mechanism. The extraction efficiency was 4.36%, indicating that the photocatalytic procedure did not affect that extraction efficiency. These findings in Figure 4 demonstrated that the number of nanomaterials used significantly impacted the efficacy of Cr (VI) elimination. The extraction efficiencies in the dark and photocatalyst processes were 7.36% and 31.26%, respectively, when the nanomaterials concentration was 0.231 g/L, as shown in the Fig. 5. As we increased the dosages (0.6 g/L), the effectiveness of the engineers' processes for producing and desorbing nanoparticles increased. A detailed examination of the findings and patterns in ecotypes reveals that increasing

the dosage between 0.135 and 0.5 g/L improves photocatalytic performance by 81% and adsorption performance by %. The discrepancy in photocatalysts' effectiveness was due to the large capability of nanoparticles' photocatalytic performance in lowering chromium (VI). The findings of this investigation were similarly reviewed by Jasrotia *et al.* (2025). It is critical to establish the least quantity of catalysts needed to achieve maximal elimination of a substance (Thangavelu et al., 2022; Chen et al., 2017).

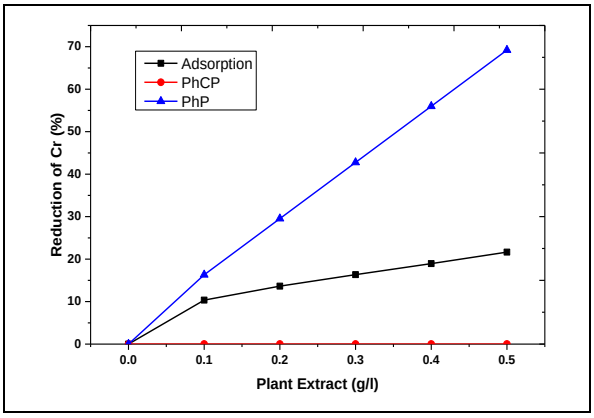

Fig. 5: The impact of Plant extract on catalytic potential

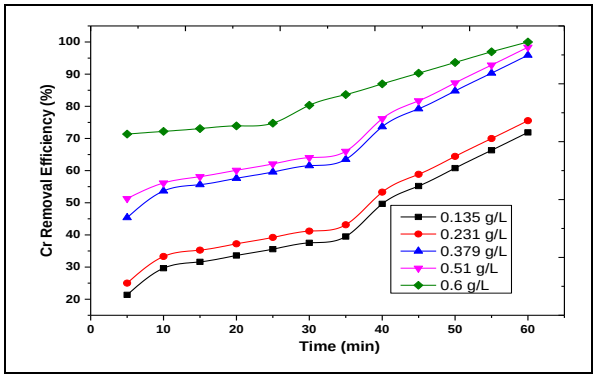

Fig. 6: The impact of plant extract concentration based on time

As a result, the influence of nanoparticle dose on Cr (VI) percentage removal was studied for 60 minutes on a specimen with a level of 40 mg/ml. As illustrated in Figure 5, 100% Cr (VI) elimination happened at all doses; nevertheless, as the amount increased, the time required to achieve 100% efficiency decreased dramatically. For example, Cr (VI) was eliminated within 60 minutes (at a dose of 0.135 g/L). The duration necessary to achieve 100% effectiveness decreased progressively as the dose was increased. Cr (VI) elimination happened after 5 minutes at a dose of 0.715 g, indicating that the inclusion of nanoparticle catalysis had a considerable influence on the Cr (VI) catalytic reaction. Modifications in the dose of different extracts used to have a substantial impact on the speed and quantity of Cr (VI) elimination, according to the data.

When the dose of the bioactive compound was increased, the number of active sites available for photocatalysis may have increased. As the number of catalyst surfaces increased, so did the amount of energised protons in the crude extract bandgap. Finally, the increased Cr (VI) renewal rate results in a shorter duration. Several studies have investigated the effect of catalytic dose on percentage removal. The results show that using more catalysts increased extraction efficiency; however, after a while, increasing the dose stabilised the efficiency (Naghizadeh *et al.* 2020).

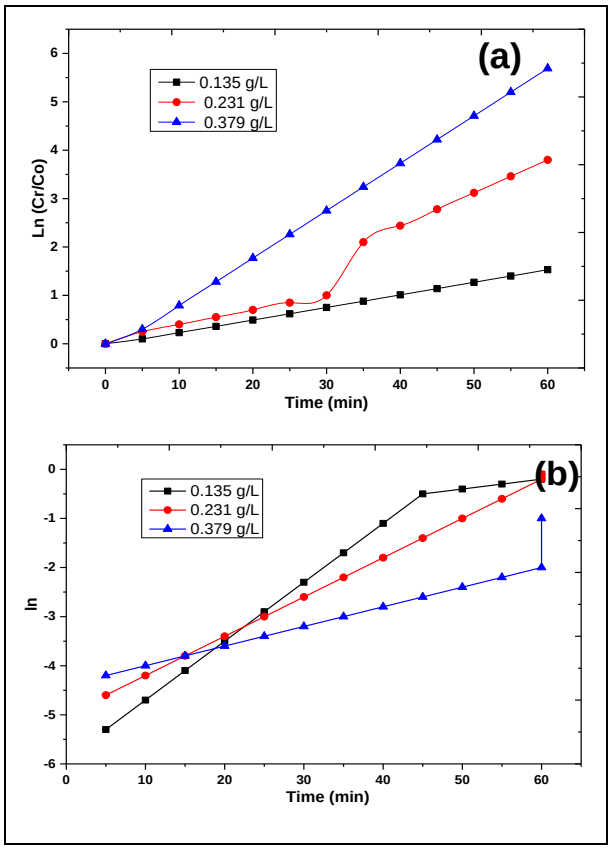

Fig. 7: Photocatalytic reduction of Cr (a) Pseudo-first-order; (b) Pseudo-second-order

Furthermore, as seen in the graphic, these latest results differed from previous investigations. The frequency of elimination rose dramatically as the quantity of bioactive compounds improved, which could be attributed to the particle's enzymatic impact and high reducing capability. The reported decrease in efficiency was linked to electricity produced by visible rays.

3.4. Kinetic Limitations of Cr (VI) Reduction

As demonstrated in Figure 6, expanding the amount of a bioactive compound substantially influenced both the first- and second-order enthalpy change characteristics. Using the estimation coefficient (R^2), The second-order response was more compatible given the laboratory results (higher R^2). As a consequence, the

dynamics of the photocatalyst for Cr (VI) elimination at various durations and doses of nanoparticles were pseudo-second-order as well as suitably compatible with this theory (R2 > 0.96). Figure 6 depicts the variations in the equilibrium constants as a function of the catalytic dose.

The connection was continuous, as could be observed, and raising the dose of fruit extracts led to a rise in the characteristic of Cr (VI) which then gradually decreased. As a result, the reaction constants were 0.082, 0.409, 0.462, and 0.425 min 1 for concentrations of 0.131, 0.335, 0.445, and 0.7 g/L, respectively. Changing the nanoparticle dosage may considerably boost the reaction rate, hence the effectiveness of a photocatalyst's Cr (VI) catalytic cycle. Those results matched those of other investigations.

3.5. Consequence of the Preliminary Meditation of Cr (VI)

The influence of a starting concentration of Cr (VI) upon that decrease in chromium at a response time of ten minutes is shown in Figure 7 and Figure 8. At this step, 0.375 g/L of nanoparticles were utilized. The increase in Cr (VI) concentration, as indicated in Figure 7, had a substantial influence on the photodegradation mechanism. By raising the starting quantity of Cr (VI) from 5 mg/L to 210 mg/L, the photocatalysts' system efficiency increased from 97.58% to 26.31%. To support these findings, it can be stated that at lower Cr (VI) concentrations, the number of photocatalytic sites accessible as well as the number of electrons generated were more significant than the number of Cr(VI) particles (Zhou *et al.* 2016; Iqbal *et al.* 2019).

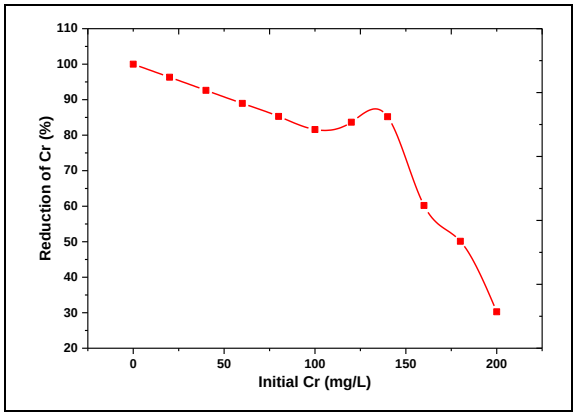

Fig. 8: Impact of initial concentration of Cr

As a result, the frequency of photocatalyst was increased significantly, and a more significant amount of Cr (VI) was eliminated. The accessible sites became progressively constrained and overloaded with bichromate particles as the starting content of Cr (VI) was increased at a consistent dose (Cai *et al.* 2020). As a result, the enthalpy change slowed, and a smaller quantity of Cr (VI) converted to Cr (III) over time. Furthermore, reducing the contaminants reduced the amount of sunlight captured on the catalysts' surfaces. The reducing effectiveness was reduced because the power of photon absorption was insufficient to produce high formation rates. The results of this research were consistent with the findings of Wu et al.'s research.

4. CONCLUSION

This work aimed to use seed extract as a sustainable and environmentally friendly source of limited reduction and stabilising agents in the green production of zero-valent metallic nanoparticles. Rc. Plant extract had a spherical shape, was homogenous, and had a 20–40 nm diameter. Their findings also showed that Rc. Plant extract had a structure that safeguarded the nanomaterials from oxidizing. The XRD data revealed the existence of metal and phenolic substituent components (nitrogen and oxide) in the formation of nanomaterials. The current study demonstrated that emerald nanostructured materials produced from seed extract seriously impacted the photocatalysts' elimination of Cr (VI), with 100% of the chromium (40 mg/l) removed in just 10 minutes. This pseudo-second degree explains the kinetics. Its substrate concentration of photocatalyst reductions rose from 0.09 to 0.5 when the catalyst's dose was raised from 0.135 g/L to 0.6 g/L, suggesting the immense promise of Cr(VI).

4.1 Future Scope

This research demonstrates the potential of seed extract in the green synthesis of zero-valent metallic nanoparticles with significant environmental benefits. Future studies could explore optimizing the extraction process and scaling up for industrial applications. Investigating the use of different plant extracts and their impact on nanoparticle size, shape, and functionality may lead to more efficient synthesis methods. Further, expanding the application of these nanoparticles in other environmental contaminants, such as heavy metals or organic pollutants, could enhance their role in sustainable water treatment. Research on the long-term stability and reusability of these nanoparticles in real-world conditions will also be critical for their practical implementation. Finally, integrating these nanomaterials into larger-scale catalytic systems or hybrid technologies may provide innovative solutions for environmental remediation.

ETHICS APPROVAL AND CONSENT TO PARTICIPATE

The research conducted in this study adhered to the ethical guidelines of the Journal. All participants provided informed consent to participate in this research. Informed consent was obtained in writing from all

participants, and they were informed about the purpose of the study, potential risks, and their rights to withdraw their participation at any time without consequence.

AVAILABILITY OF DATA AND MATERIALS

The data used to support the findings of this study are included within the article. Should further data or information be required, these are available from the corresponding author upon request.

FUNDING

This research received no specific grant from any funding agency in the public, commercial, or not-for-profit sectors.

CONFLICTS OF INTEREST

The authors declare that there is no conflict of interest.

COPYRIGHT

REFERENCES

Cai, C., Teng, Y., Wu, J. H., Li, J. Y., Chen, H. Y., Chen, J. H. and Kuang, D. B., In situ photosynthesis of an MAPbI3/CoP hybrid heterojunction for efficient photocatalytic hydrogen evolution, *Adv. Funct. Mater.*, 30(35), 2001478 (2020). https://doi.org/10.1002/adfm.202001478

Chen, X., Chen, H., Guan, J., Zhen, J., Sun, Z., Du, P. and Yang, S., A facile mechanochemical route to a covalently bonded graphitic carbon nitride (gC_3N_4) and fullerene hybrid toward enhanced visible light photocatalytic hydrogen production, *Nanoscal*e, 9(17), 5615-5623 (2017). https://doi.org/10.1039/C7NR01237C

FOpoku, F., Govender, K. K., Van Sittert, C. G. C. E. and Govender, P. P., Recent progress in the development of semiconductor-based photocatalyst materials for applications in photocatalytic water splitting and degradation of pollutants, *Adv. Sustain. Syst.*, 1(7), 1700006 (2017). https://doi.org/10.1002/adsu.201700006

Gupta, V. K., Pathania, D., Asif, M. and Sharma, G., Liquid phase synthesis of pectin–cadmium sulfide nanocomposite and its photocatalytic and antibacterial activity, *J. Mol. Liq.*, 196, 107-112 (2014). https://doi.org/10.1016/j.molliq.2014.03.021

Haldorai, Y. and Shim, J. J., Multifunctional chitosan-copper oxide hybrid material: Photocatalytic and antibacterial activities, *Int. J. Photoenergy.*, (1), 245646 (2013). https://doi.org/10.1155/2013/245646

Huang, Y., Lu, Y., Lin, Y., Mao, Y., Ouyang, G., Liu, H. and Tong, Y., Cerium-based hybrid nanorods for synergetic photo-thermocatalytic degradation of organic pollutants, *J. Mater. Chem. A.*, 6(48), 24740-24747 (2018). https://doi.org/10.1039/C8TA06565A

Iqbal, T., Ali, F., Khalid, N. R., Tahir, M. B. and Ijaz, M., Facile synthesis and antimicrobial activity of CdS-Ag_2S nanocomposites, *Bioorg Chem.*, 90, 103064 (2019). https://doi.org/10.1016/j.bioorg.2019.103064

Jasrotia, R., Prakash, J., Saddeek, Y. B., Alluhayb, A. H., Younis, A. M., Lakshmaiya, N., & Sharma, P., Cobalt ferrites: Structural insights with potential applications in magnetics, dielectrics, and Catalysis, *Coord. Chem. Rev*., 522, 216198 (2025). https://doi.org/10.1016/j.ccr.2024.216198

Jiang, J., Pi, J. and Cai, J., The advancing of zinc oxide nanoparticles for biomedical applications, *Bioinorg. Chem. Appl.*, 2018(1), 1062562 (2018). https://doi.org/10.1155/2018/1062562

Mekatel, H., Amokrane S., Bellal, B., Trari, M. and Nibou, D., Photocatalytic reduction of Cr(VI) on nanosized Fe2O3 supported on natural Algerian clay: Characteristics, kinetic and thermodynamic study, Biochem. Eng. J., 200, 611-618(2012). https://doi.org/10.1016/j.cej.2012.06.121

Naghizadeh, A., Mohammadi-Aghdam, S. and Mortazavi-Derazkola, S., Novel $CoFe_2O_4$@ ZnO-CeO_2 ternary nanocomposite: Sonochemical green synthesis using Crataegus microphylla extract, characterization and their application in catalytic and antibacterial activities, *Bioorg Chem.*, 103, 104194 (2020). https://doi.org/10.1016/j.bioorg.2020.104194

Nassar, M. Y., Ahmed, I. S. and Samir, I., A novel synthetic route for magnesium aluminate ($MgAl_2O_4$) nanoparticles using sol–gel auto combustion method and their photocatalytic properties, *Spectrochim. Acta A Mol. Biomol. Spectrosc.*, 131, 329-334 (2014). https://doi.org/10.1016/j.saa.2014.04.040

Nguyen, V. H., Nguyen, B. S., Jin, Z., Shokouhimehr, M., Jang, H. W., Hu, C. and Van Le, Q., Towards artificial photosynthesis: Sustainable hydrogen utilization for photocatalytic reduction of CO_2 to high-value renewable fuels, *Chem. Eng. J.*, 402, 126184 (2020). https://doi.org/10.1016/j.cej.2020.126184

Omar, F. S., Nay Ming, H., Hafiz, S. M. and Ngee, L. H., Microwave synthesis of zinc oxide/reduced graphene oxide hybrid for adsorption-photocatalysis application, *Int. J. Photoenergy*, 2014(1), 176835 (2014). https://doi.org/10.1155/2014/176835

Onwumere, J., Piątek, J., Budnyak, T., Chen, J., Budnyk, S., Karim, Z. and Slabon, A., CelluPhot: hybrid Cellulose− Bismuth oxybromide membrane for ollutant removal, *ACS Appl. Mater. Interfaces*, 12(38), 42891-42901 (2020). https://doi.org/10.1021/acsami.0c12739

Samadi, Z., Yaghmaeian, K., Mortazavi-Derazkola, S., Khosravi, R., Nabizadeh, R. and Alimohammadi, M., Facile green synthesis of zero-valent iron nanoparticles using barberry leaf extract (GnZVI@ BLE) for photocatalytic reduction of hexavalent chromium, *Bioorg Chem.*, 114, 105051 (2021). https://doi.org/10.1016/j.bioorg.2021.105051

Thangavelu, L., Veeraragavan, G. R., Mallineni, S. K., Devaraj, E., Parameswari, R. P., Syed, N. H. and Bhawal, U. K., [Retracted] Role of Nanoparticles in Environmental Remediation: An Insight into Heavy Metal Pollution from Dentistry, *Bioinorg. Chem. Appl.*, 2022(1), 1946724 (2022). https://doi.org/10.1155/2022/1946724

Wang, Q., Yun, G., Bai, Y., An, N., Lian, J., Huang, H. and Su, B., Photodegradation of rhodamine B with $MoS_2/Bi_2O_2CO_3$ composites under UV light irradiation, *Appl. Surf. Sci.*, 313, 537-544 (2014). https://doi.org/10.1016/j.apsusc.2014.06.018

Zangeneh, H., Zinatizadeh, A. A., Zinadini, S., Feyzi, M. and Bahnemann, D. W., Preparation and characterization of a novel photocatalytic self-cleaning PES nanofiltration membrane by embedding a visible-driven photocatalyst boron doped-$TiO_2SiO_2/CoFe_2O_4$ nanoparticles, *Sep Purif Technol.*, 209, 764-775 (2019). https://doi.org/10.1016/j.seppur.2018.09.030

Zhang, C., Li, Y., Shuai, D., Shen, Y., Xiong, W. and Wang, L., Graphitic carbon nitride (g-C_3N4)-based photocatalysts for water disinfection and microbial control: A review, *Chemosphere*, 214, 462-479 (2019). https://doi.org/10.1016/j.chemosphere.2018.09.137

Zhao, Y., Jia, X., Waterhouse, G. I., Wu, L. Z., Tung, C. H., O'Hare, D. and Zhang, T., Layered double hydroxide nanostructured photocatalysts for renewable energy production, *Adv. Energy Mater.*, 6(6), 1501974 (2016). https://doi.org/10.1002/aenm.201501974

Zhou, H., Yan, R., Zhang, D. and Fan, T., Challenges and perspectives in designing artificial photosynthetic systems, *Chem. Eur. J.*, 22(29), 9870-9885 (2016). https://doi.org/10.1002/chem.201600289